HHS Public Access

Author manuscript

Matter. Author manuscript; available in PMC 2020 October 02.

Published in final edited form as:

Matter. 2019 October 2; 1(4): 926–944. doi:10.1016/j.matt.2019.07.019.

An Antimicrobial Dental Light Curable Bioadhesive Hydrogel for Treatment of Peri-Implant Diseases

Ehsan Shirzaei Sani[1], **Roberto Portillo Lara**[2], **Zahra Aldawood**[3], **Seyed Hossein Bassir**[3,4], **Daniel Nguyen**[5], **Alpdogan Kantarci**[5], **Giuseppe Intini**[6,7,8], **Nasim Annabi**[1,9,10,*]

[1]Chemical and Biomolecular Engineering Department, University of California -Los Angeles, Los Angeles, CA 90095, USA.

[2]Tecnologico de Monterrey, Escuela de Ingeniería y Ciencias, Zapopan, JAL 44-49, México.

[3]Department of Oral Medicine, Infection, and Immunity, Harvard School of Dental Medicine, Boston, MA 02115, USA.

[4]Department of Periodontology, School of Dental Medicine, Stony Brook University, Stony Brook, NY 11794, USA.

[5]Department of Applied Oral Sciences, The Forsyth Institute, Cambridge, MA 02142, USA.

[6]Department of Periodontics and Preventive Dentistry, University of Pittsburgh, School of Dental Medicine, Pittsburgh, PA 15213, USA.

[7]McGowan Institute for Regenerative Medicine, University of Pittsburgh, Pittsburgh, PA 15213, USA

[8]Harvard Stem Cell Institute, Harvard University, Cambridge, MA 02115, USA.

[9]Center for Minimally Invasive Therapeutics (C-MIT), California NanoSystems Institute (CNSI), University of California -Los Angeles, Los Angeles, CA 90095, USA.

[10]Lead Contact

[*]Corresponding author: N. Annabi, address: nannabi@ucla.edu.

AUTHOR CONTRIBUTIONS

Ehsan Shirzaei Sani, N.A., G.I., and A.K. designed the experiments. Ehsan Shirzaei Sani synthesized the bioadhesive hydrogels. Ehsan Shirzaei Sani conducted the physical characterization and adhesion experiments. Ehsan Shirzaei Sani conducted the *in vitro* cytocompatibility tests. Ehsan Shirzaei Sani and D.N. performed the *in vitro* antimicrobial test. Ehsan Shirzaei Sani, R.P.L., and S.H.B. extracted and encapsulated the calvarial bone sutures. Ehsan Shirzaei Sani and Z.A. conducted the *in vivo* experiments, and Ehsan Shirzaei Sani performed histopathological analysis. All the authors contributed to the interpretation of the results and data analysis. The paper was written by Ehsan Shirzaei Sani and R.P.L. and was revised and corrected by N.A., G.I., and A.K.. The project was supervised by N.A.

SUPPORTING INFORMATION

Supporting Information can be found online at Cell Press.

DECLARATION OF INTERESTS

Ehsan Shirzaei Sani and N.A. are inventors on a U.S. Provisional Patent Application (No. 62/860,939), entitled “Osteoinductive modified gelatin hydrogels and methods of making and using the same”, filed by UCLA’s Technology Development Group (TDG) with the United States Patent and Trademark Office (USPTO). The other authors declare no competing interests.

SUMMARY

Dental implants constitute the standard of care to replace the missing teeth, which has led to an increase in the number of patients affected by peri-implant diseases (PIDs). Here, we report the development of an antimicrobial bioadhesive, GelAMP, for the treatment of PIDs. The hydrogel is based on a visible light-activated naturally-derived polymer (gelatin) and an antimicrobial peptide (AMP). The optimized formulation of GelAMP could be rapidly crosslinked using commercial dental curing systems. When compared to commercial adhesives, the bioadhesives exhibited significantly higher adhesive strength to physiological tissues and titanium. Moreover, the bioadhesive showed high cytocompatibility and could efficiently promote cell proliferation and migration *in vitro*. GelAMP also showed remarkable antimicrobial activity against *Porphyromonas gingivalis*. Furthermore, it could support the growth of autologous bone after sealing calvarial bone defects in mice. Overall, GelAMP could be used as a platform for the development of more effective therapeutics against PIDs.

eTOC blurb

Dental implants are the current solution for replacing of the missing teeth. However, majority of the patients with implants suffer from implant diseases caused by microbial infection and bone loss. There is an unmet need for the treatment of dental diseases. We developed a safe, cheap, and fast applicable glue with antimicrobial properties, designed for the treatment of periodontal diseases. This material can be delivered in liquid form around the implant and solidified by using a dental light to prevent infection and promote bone healing.

Graphical Abstract

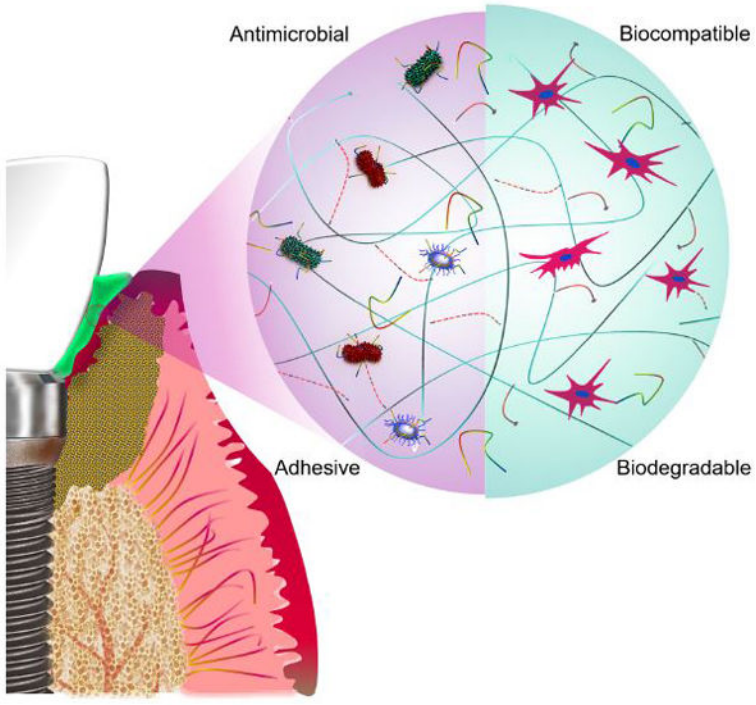

Keywords

Peri-implant diseases; antimicrobial hydrogels; tissue adhesive

1. INTRODUCTION

As dental implants have become the standard of care for replacement of the missing teeth, the number of patients affected by peri-implant diseases (PIDs) is increasing[1]. According to their clinical manifestations, PIDs can be mainly categorized in peri-implant mucositis (PIM) and peri-implantitis (PI)[2]. PIM refers to a reversible inflammatory process that affects the soft tissues surrounding an implant, resulting in bleeding on gentle probing, and in some cases, suppuration, erythema, and swelling[2]. The etiology of PIM is the bacterial accumulation and biofilm formation around the dental implant[3]. On the other hand, PI presents not only with inflammation of the soft tissues but is also accompanied by a progressive bone loss that could lead to implant failure [4] Clinical data has shown that progression from PIM to PI is strongly associated with lack of preventive maintenance and thus, opportune treatment of PIM could prevent the progression to PI [5].

Currently, PIM can be treated with nonsurgical procedures, which include mechanical debridement, alone or in combination with local delivery of antibiotics such as Arestin (minocycline HCL), Elyzol® (metronidazole 25%), and Atridox® (doxycycline hyclate 10%) which can be injected directly into the sulcus or peri-implant pockets [6; 7] However, because of their inability to efficiently antagonize the infection[8], the therapeutic efficacy of these approaches is limited [9]. In addition, local and systemic administration of antibiotics may result in hypersensitivity reactions in allergic patients, as well as the development of antibiotic-resistant strains of pathogenic bacteria [10; 11]. Moreover, as the number of dental implants being placed has continue to increase worldwide; it is predicted that PIDs will become one of the most prominent dental diseases of the future[3]. Therefore, there is a need for more effective therapeutic strategies that could be used to prevent bacterial growth and promote healing around dental implants for the treatment of PIDs.

Current treatments against PIM are mainly aimed at eradicating subgingival dysbiosis and restoring homeostasis to microbial communities in the oral cavity[12]. However, clinical data has shown that nonsurgical mechanical approaches, aimed at disinfection of the affected area, often fail due to recolonization of the periodontal or peri-implant pockets by pathogenic bacteria that perpetuate the disease [12; 13]. Moreover, bacterial infection and the subsequent epithelial cell death lead to the release of inflammatory cytokines and chemotactic bacterial peptides, which attract migratory neutrophils that could worsen implant prognosis. This is mainly because neutrophil degranulation due to bacterial overload releases tissue-degrading enzymes into the gingival crevice that lead to further tissue trauma [14; 15]. As inflammation extends from the marginal gingiva into the supporting periodontal tissues, PIM could eventually progress to PI and lead to bone loss and implant failure. Therefore, therapeutic strategies that efficiently isolate the affected area to prevent the infiltration of bacteria and other unwanted cells, while also enabling the growth of bone-

competent cells (i.e., compartmentalized tissue healing) could improve the clinical outcome of patients with PIDs [16; 17]

Periodontal regeneration requires the hierarchical and coordinated response of a variety of soft and hard tissues (i.e., periodontal ligament, gingiva, cementum, and bone) during the wound healing process[18]. In recent years, clinical evidence has shown that treatment options based on resorbable and non-resorbable membranes could be used for guided tissue regeneration of the periodontal tissues affected by PIDs[19]. Current third-generation membranes are developed not only to act as passive barriers but also as delivery vehicles for the release of specific antibiotics and growth factors [20; 21]. Moreover, local delivery yields higher local concentrations of the therapeutic agents, which increases the effectiveness at the site and decreases the risk of systemic side effects. However, several limitations remain pertaining to the unpredictability of the efficacy of these treatments and the need for the delivery multiple biological mediators to promote tissue regeneration[22;23].

Hydrogel-based bioadhesives hold remarkable potential for soft and hard tissue engineering applications due to their tunable composition and physical properties. The precise control over the microarchitecture, mechanical properties and degradation rate of hydrogels, make them great alternatives for the controlled delivery of a variety of therapeutic agents *in vivo*. For instance, our group has previously reported the development of antimicrobial hydrogel adhesives for the treatment of chronic non-healing wounds [24] and orthopedic applications [25], which were based on extracellular matrix (ECM)-derived biopolymers. In the field of regenerative dentistry, previous studies have reported the engineering of hydrogels based on the combination of alginate with the soluble and insoluble fractions of the dentin matrix [26] More recently, other groups have developed cell-laden gelatin-based hydrogels that could be photopolymerized using dental curing lights [27] However, to the best of our knowledge, the development of antimicrobial hydrogels that can strongly adhere to hard and soft oral surfaces for the treatment of PIDs has not been reported.

Here, we describe the development of a visible light-crosslinkable antimicrobial hydrogel adhesive for the treatment of PIDs. This bioadhesive was engineered through the incorporation of a cationic AMP (Tet213) into a photocrosslinkable gelatin methacryloyl hydrogels to form gelatin methacryloyl-antimicrobial peptide (GelAMP) bioadhesives. We characterized the physical and the adhesive properties of the bioadhesives *in vitro*. We also evaluated the antimicrobial properties of the bioadhesives against *Porphyromonas gingivalis* (*P. gingivalis*), a Gram-negative bacterium that is involved in the pathogenesis of PIDs. The cytocompatibility of the bioadhesives was also evaluated *in vitro* via two-dimensional (2D) surface seeding and three-dimensional (3D) encapsulation of W-20–17 murine fibroblasts. Lastly, we evaluated the ability of the bioadhesives to support bone regeneration *in vivo* using a calvarial defect model in mice. The engineered antimicrobial bioadhesives could constitute an effective approach to prevent bacterial growth, while also supporting tissue regeneration for the treatment of PIDs.

2. RESULTS AND DISCUSSION

2.1. Synthesis and physical characterization of the adhesive hydrogels

The GelAMP bioadhesives were synthesized based on the combination of biocompatible photoinitiators (triethanolamine (TEA)/N-vinyl caprolactam (VC)/Eosin Y), a naturally-derived gelatin-based biopolymer (gelatin methacryloyl), and an antimicrobial peptide (AMP tet213). Type I or cleavage-type initiators are widely used in tissue engineering and are designed to be activated within the range of UV wavelength (i.e. 360–400 nm). However, exposure to UV light could lead to cell and damage [28], impair cellular function [29], and even lead to neoplasia and cancer [30]. Moreover, only a few type I photoinitiators such as 2-Hydroxy-4′-(2-hydroxyethoxy)-2-methylpropiophenone (Irgacure-2959) and Lithium phenyl-2,4,6-trimethylbenzoylphosphinate (LAP) have been shown to be cytocompatible at low concentrations [30–32]. However, Irgacure-2959 has low water solubility and cannot be activated with visible light since its molar absorptivity is limited in the visible light range (wavelengths > 400 nm). Although LAP has high water solubility and cytocompatibility, its highest molar absorbance is in UV range wavelengths (365 – 385 nm, $\varepsilon \approx 150 – 230\ M^{-1}\ cm^{-1}$), which limits its activation in the visible light range ($\varepsilon \approx 30\ M^{-1}\ cm^{-1}$ at 405 nm)[33]. Considering the effective wavelength of Food and Drug Administration (FDA) approved dental curing light systems (420 – 480 nm), cleavage-type photoinitiators have limited potential to be used with these platforms in the clinical setting. To address these limitations, we used a visible light activated photoinitiator, Eosin Y, which is known as Type II or noncleavage-type photoinitiator. This photoinitiator not only can minimize the safety concerns associated with UV light, but also can be rapidly activated with wavelengths (420 – 480 nm, $\varepsilon > 50000\ M^{-1}\ cm^{-1}$) produced by commercial dental curing systems [33; 34] TEA and VC were used as a co-initiator and a co-monomer respectively, to assist free radical photoinitiation [34].

Hydrogels were synthesized using the highly cytocompatible and visible-light activated polymer gelatin methacryloyl, a chemically modified form of hydrolyzed collagen that possesses a high number of cell binding motifs and matrix-metalloproteinase (MMP) degradation sites [31]. These characteristics are critical to ensure proper cell attachment and colonization of the scaffold. Lastly, we incorporated the AMP Tet213 into the bioadhesive precursor to impart antimicrobial properties to the hydrogels. AMPs do not readily lead to the selection of resistant mutants and are effective at very low concentrations, which makes them ideal candidates to prevent bacterial growth in biomedical implants via local delivery[35]. To form the antimicrobial GelAMP bioadhesives, the prepolymers were dissolved at various concentrations (7% and 15%) in a photoinitiator solution containing Tet213 (0.2% (w/v), or 1.34 mM) and photocrosslinked using a dental curing light (420 – 480 nm) (Fig. 1A). Control hydrogels, Gel, were formed using a similar technique, but without incorporation of AMP.

To evaluate the physical properties of the bioadhesives, hydrogel formulations were synthesized based on two different concentrations of bioadhesive (7 and 15% (w/v)) with and without incorporation of AMP. Our results showed that 15% (w/v) bioadhesive hydrogels exhibited a 4.3-fold and 3.2-fold increase in the compressive and elastic moduli,

respectively, when compared to 7% (w/v) hydrogels (Fig. 1B). In addition, the extensibility of the bioadhesives did not change by changing the concentration of bioadhesive from 7% to 15% (w/v) or by the addition of AMP (Fig. 1C). However, the ultimate tensile strength of hydrogels increased from 5.2 ± 1.3 kPa to 19.8 ± 3.5 kPa as the bioadhesive concentration was increased from 7% to 15% (w/v) (Fig. 1D). The results also showed that the addition of AMP did not alter the mechanical properties of the bioadhesives, which could be due to the low concentration and the small size of the AMP [24].

Next, we examined the *in vitro* stability of the bioadhesives by incubating them in collagenase type II solution in DPBS (20 μg/ml) for 5 days. Bioadhesives with 7% (w/v) concentration resulted in significantly accelerated degradation as compared to bioadhesives with 15% (w/v) concentration. In particular, the 7% (w/v) bioadhesive showed 100.0 % degradation by day 5 post-incubation, while 29.4 ± 2.2 % of the hydrogel with 15% (w/v) concentration was degraded during the same time (Fig. 1E). In addition, there was no significant difference in the degradation of bioadhesive hydrogels with or without AMP (Fig. 1E).

The *in vivo* biodegradation of GelAMP bioadhesive was also confirmed in a rat subcutaneous implantation model. Accordingly, hematoxylin and eosin (H&E)) analysis of the explanted samples revealed a significant deformation and biodegradation of hydrogels after 56 days of implantation when compared to day 7 (Fig. S4). This can be mainly due to the enzymatic hydrolysis of the gelatin backbone [25].

We then determined the water uptake capacity of the hydrogels, by calculating the swelling ratios of the bioadhesives at different concentrations and time points. For this, the swelled weights of the samples after incubation at 37 °C in DPBS was divided by their corresponding dry weights. As shown in Fig. 1F, the swelling ratios of the hydrogels decreased by increasing bioadhesive concentrations. However, the swelling ratios barely changed after 10 h of incubation, indicated that the equilibrium states were achieved at this time point. In addition, the incorporation of AMP did not alter the degradation rate and the swellability of the bioadhesives (Fig. 1E, F). Overall, bioadhesives with 15% (w/v) concentration showed higher mechanical stiffness and slower degradation rates as compared to 7% (w/v) hydrogels. Previous studies have also studied the effect of physical properties and microstructural features of hydrogel scaffolds on the regeneration and repair of target tissues[24; 36]. An ideal bioadhesive used in the setting of the oral cavity should be elastic and flexible, as well as sufficiently strong to withstand breakage due to the intrinsic dynamism of the oral tissues [37]. For this purpose, the water uptake capacity of the bioadhesives should be finely tuned to prevent excessive swelling, which could lead to patient discomfort and detachment from the wet and highly motile oral tissues. Furthermore, fast degradation of the adhesive could compromise adequate retention and greatly limit their clinical efficacy [24] Our results showed that, in addition to the higher modulus (Fig. 1B), and ultimate strength (Fig. 1D) of the 15% (w/v) bioadhesives, they also showed comparatively higher structural stability *in vitro*. This was demonstrated by their slower degradation rates (Fig. 1E) and similar swelling equilibrium states upon incubation in DPBS (Fig. 1F) when compared to 7% (w/v) bioadhesives. Next, we evaluated the adhesive properties of the hydrogels to soft physiological tissues and hard implant surfaces.

2.2. In vitro and ex vivo characterization of the adhesive properties

The strong retention and adhesion of biomaterials to both the native tissue and the implant surface is a critical factor to promote periodontal tissue repair and regeneration[38]. Moreover, the designed bioadhesive must withstand the shear and the pressure exerted by the underlying tissues and the high motility of the oral tissues. To evaluate these parameters, we performed standard *in vitro* adhesion tests including wound closure (ASTM F2458–05), lap shear (ASTM F2255–05), and burst pressure (ASTM F2392–04) to assess the adhesiveness of the hydrogels to physiological tissues and titanium surfaces. Similar tests were also performed using a commercially available sealant, CoSEAL™, as control. Wound closure tests were performed to measure the adhesive strength of the bioadhesives to soft tissues including porcine gingiva (Fig. 2A, B) and porcine skin (Fig. S1). The results of the wound closure tests revealed that the adhesive strength of the hydrogel to gingiva increased from 23.5 ± 5.4 kPa to 55.3 ± 6.7 kPa, by increasing the hydrogel concentration from 7 to 15% (w/v) (Fig. 2B). Similarly, the adhesive strength of the bioadhesives to porcine skin was increased 2.1-fold by increasing the total polymer concentration from 7 to 15% (w/v) (Fig. S1). Moreover, the presence of AMP did not alter the adhesion strength of the hydrogels for both porcine gingiva and skin (Fig. 2B, Fig. S1). Lastly, the adhesive strength of the 15% (w/v) bioadhesive was significantly higher than that of CoSEAL™, with a 3.3-fold difference for gingiva tissue and a 1.7-fold difference for skin tissue (Fig. 2B and Fig. S1).

Similar to the wound closure tests, 15% (w/v) bioadhesives, with and without AMP, showed significantly higher lap shear strength to titanium surface as compared to CoSEAL™ (i.e., 3.7 and 4.6-fold difference, respectively) (Fig. 2D). However, the lap shear strength did not significantly change for 15% (w/v) bioadhesives with and without AMP (Fig. 2D). In contrast, the burst pressure of the bioadhesives was increased from 17.0 ± 2.9 kPa at 7% (w/v) to 34.6 ± 4.0 kPa at 15% (w/v) final polymer concentration. Furthermore, the highest burst pressure was observed for 15% (w/v) hydrogels (37.7 ± 6.5 kPa), which was significantly higher than that of CoSEAL™ (1.7 ± 0.1 kPa) (Fig. S2).

Different hydrogel adhesives have been used for sealing, reconnecting tissues, or as implant coatings [38; 39] However, their poor mechanical properties and adhesion to wet tissues have limited their implementation in the clinic. Moreover, the majority of the commercially available dental adhesives are based on polymethyl methacrylate (PMMA) or acrylic based resins, which are mainly used as fillers for dentin cavities. Although these types of adhesives have shown strong adhesion and binding to the oral surfaces and tissues (i.e., gingiva and pulpal walls), their potential as a platform for the treatment of PIDs is limited [40; 41]. This is mainly due to the lack of cell-binding sites, and poor tissue biointegration, which ultimately limit the regenerative capacity of these resins [41]. In contrast, our results revealed that our visible light curable bioadhesives are able to bind strongly to both hard (titanium) and soft (gingiva) surfaces and withstand high shear stress and pressure. In addition, we have previously shown that gelatin-based bioadhesives can strongly adhere to wet and dynamic tissues such as the lungs [31]. Therefore, these bioadhesives could be used to effectively adhere to periodontal tissues, as well as under palatal pressure and during mastication. Moreover, due to the high regenerative capacity of ECM-derived biopolymers, gelatin-based bioadhesives could constitute a suitable alternative for the treatment of PIDs [24]

2.3. In vitro evaluation of the antimicrobial properties of the bioadhesives

AMPs are comprised of short sequences of cationic amino acids, which have been shown to possess broad spectrum bactericidal activity against both normal and antibiotic resistant bacteria [24; 35]. AMPs bind to the negatively charged outer leaflet of bacterial cell membranes, which leads to changes in bacterial surface electrostatics, increased membrane permeabilization, and cell lysis [24].

Here, we synthesized GelAMP, a dental light curable bioadhesive with antimicrobial properties through the incorporation of AMP into bioadhesive hydrogels. Previously, we have shown that AMP tet213 at very low concentrations is effective against both G (+/−) bacteria [24] Here, we used an optimized concentration of AMP in this work (0.2 %(w/v)) based on our previous study [24]. First, we evaluated the antimicrobial activity of the resulting bioadhesive against *P. gingivalis* using a standard colony forming units (CFU) assay and direct visualization of the bacteria-laden hydrogels via scanning electron microscope (SEM) (Fig. 3). The CFU assay showed that the number of *P. gingivalis* colonies in the 3-logarithmic dilution decreased from 37.7 ± 3.5 at 0.0% (w/v) AMP, to 10.6 ± 1.9 at 0.2% (w/v) AMP (Fig. 3A, B). A similar response was also observed for the 4-logarithmic dilution, which further confirmed the bactericidal properties of the engineered antimicrobial GelAMP bioadhesives, when compared to pristine hydrogels as controls (Fig. 3B). SEM micrographs also showed that the hydrogels without AMP exhibited significant bacterial infiltration and colonization throughout the polymer network (Fig. 3C). In contrast, GelAMP containing 0.2% (w/v) AMP, showed high antimicrobial activity as demonstrated by the complete absence of bacterial clusters on both surface and cross sections of the bioadhesives (Fig. 3D).

A variety of AMPs such as defensins and cathelicidins are normally found in the oral cavity, particularly in the gingival crevicular fluid and in salivary secretions, and constitute the first line of defense against bacterial infection [42]. Moreover, AMPs do not trigger resistance mechanisms and play a key role in the regulation of microbial homeostasis and the progression of gingival and periodontal diseases [43]. Because of this, previous groups have explored the use of AMPs as active coatings for dental implants and other therapeutic strategies aimed at the prevention of bacterial infection [44; 45]. However, AMPs are highly susceptible to proteolytic degradation by proteases secreted by bacteria and host cells and thus, efficient *in vivo* delivery of AMPs to the site of infection remains challenging. Thus, the engineered bioadhesives in this work could be used to protect AMPs from environmental degradation and to deliver physiologically relevant concentrations of AMPs for controlled periods of time.

2.4. Cell studies

An ideal bioadhesive not only must be cytocompatible but should also allow the attachment and proliferation of cells within the 3D microstructure to support biointegration and healing. Here, we assessed the ability of the engineered bioadhesives to support the attachment and proliferation of migratory cells from the bone stroma via 3D encapsulation of bone marrow stromal cells (Fig. 4). In addition, we evaluated the ability of the bioadhesives to support the

growth and proliferation of migratory stromal cells via 3D encapsulation of freshly isolated calvarial bone sutures.

***In vitro* cytocompatibility and proliferation of 3D encapsulated cells within bioadhesive hydrogels:** First, we evaluated the viability, metabolic activity, and spreading of bone marrow mouse stromal cells (W-20–17 [46]) encapsulated within the adhesives using a live/dead and PrestoBlue assays, and F-Actin/DAPI staining, respectively. Our results showed that cells encapsulated within the bioadhesives with and without AMP exhibited > 90% viability after 5 days of culture (Fig. 4A, B). In addition, the incorporation of AMP, did not affect the viability of the encapsulated cells (Fig. 4A, B). Moreover, F-Actin/DAPI staining revealed that W-20–17 cells could attach and proliferate throughout the 3D network for Gel and GelAMP adhesives, up to 5 days of culture (Fig. 4C). Furthermore, the metabolic activity of cells in GelAMP hydrogels increased consistently from 2273 ± 66 RFUs at day 1 to 10041 ± 938 RFUs at day 5 of culture (Fig. 4D). In addition, there were no statistically significant differences between the metabolic activity of cells seeded on GelAMP and Gel adhesives (Fig. 4D).

3D encapsulation of calvarial bone suture explants within bioadhesives: We encapsulated the freshly isolated calvarial bone sutures in both 7 and 15% (w/v) hydrogels to evaluate the ability of the bioadhesives to support the proliferation and migration of stromal cells (Fig. 4E). During the first week of encapsulation, no significant cell migration was observed. A week after encapsulation, cell (most likely suture-derived skeletal stem cells [47; 48]) deployment out of the suture was observed, followed by proliferation and migration within the bioadhesive hydrogel (Fig. 4F). The migratory and proliferative behavior of these cells were assessed for up to 30 days post-encapsulation (Fig. 4F). These results showed that the metabolic activity of the encapsulated cells increased consistently for both 7% and 15% (w/v) bioadhesives (Fig. 4G). For instance, the metabolic activity of the cells in 15% GelAMP (w/v) bioadhesives increased from 3016 ± 678 RFUs at day 10, to 22869 ± 3421 RFUs at day 30 post-encapsulation (Fig. 4G). However, we did not observe any statistical difference between metabolic activity of the cells seeded within the 7% and 15% (w/v) bioadhesive hydrogels (Fig. 4G).

Our results also indicated that the antimicrobial bioadhesives did not elicit any cytotoxic response and could effectively support the growth of both W-20–17 and suture-derive skeletal stem cells *in vitro*. Previous studies have reported the development of different types of antimicrobial hydrogels based on the incorporation of metal or metal oxide nanoparticles [24; 49] However, the negative effect of metal oxide nanoparticles on cell viability greatly limit their application for the clinical management of PIDs [49]. In contrast, our results remonstrated that the cells could infiltrate and spread throughout our antimicrobial bioadhesives, while also remaining proliferative and metabolically active.

Taken together, these results demonstrated that our bioadhesives could be used to form an adhesive and antimicrobial barrier that prevents bacterial growth and supports the proliferation of bone-competent cells *in vitro*. The ability of the bioadhesives to eradicate or prevent infection at the implant site could not only be relevant to disinfect the affected area, but also to reduce inflammatory responses triggered by sustained microbial colonization.

Moreover, the establishment of a cell-supportive microenvironment could promote the regeneration of the affected bone by endogenous progenitor cells that migrate into the wound site. Therefore, we next aimed to evaluate the ability of the bioadhesives to support bone regeneration *in vivo* using a calvarial defect model in mice.

2.5. In situ application and in vivo evaluation of bioadhesive hydrogels

We investigated the ability of the hydrogels to be delivered and formed *in situ* and to remain firmly attached to the wound area without the risk of displacement during the healing process. For this, we first created critically sized defects in mice calvaria using dental drills. The bioadhesive precursor solutions (7% and 15% (w/v)) were directly injected into the bone defects and photopolymerized using a commercial dental light curing unit (Fig. 5A). Our results showed that the bioadhesives could remain at the site of application without any sign of displacement after 7 and 14 days of implantation (Fig. 5B). In addition, histological assessment (H&E) showed the complete sealing of the defect and a strong coherence between the biopolymer and the native bone following application (Fig. 5C). Moreover, the H&E images also revealed that bioadhesives with both formulations (7, and 15% (w/v)) could remain attached to the wound site up to 42 days after application (Fig. 5D, E). At earlier time points (14 days post application), the formation of new autologous bone could be observed near the margin of the original defect (Fig. S3). Calvarial defects in untreated control animals showed limited new bone formation at day 42 post application (Fig. 5F). In contrast, histological staining revealed the formation of new bone for both 7% and 15% (w/v) bioadhesives (Fig. 5D, E). Furthermore, the area covered by the newly formed bone was significantly larger for defects treated with 15% (w/v) hydrogels as compared to 7% (w/v) hydrogels (Fig. S3). This observation could be explained in part due to the increased structural integrity of bioadhesives with higher polymer concentration, which provided a more structurally stable scaffold to support bone regeneration and the ingrowth of the adjacent connective tissues (Fig. 5E). These observations provided qualitative evidence that was indicative of the formation of new bone and the subsequent repair of the defect.

To perform a quantitative evaluation of new bone formation, micro-computed tomography (μCT) was performed on untreated defects, as well as defects treated with bioadhesive synthesized using 7 and 15% (w/v) polymer concentrations at days 0, 28, and 42 post-procedure (Fig. 6). Our results showed that the untreated defects exhibited limited evidence of bone forming up to 28-and 42 days post-procedure, with little decrease in the extension of the critical size (Fig. 6A). At day 28, the defects treated with the 15% (w/v) hydrogels showed significantly higher bone formation than 7% (w/v) hydrogels and the untreated controls. At day 42, a significant amount of new bone was observed for defects treated with 15% (w/v) hydrogels (Fig. 6A). In addition, on days 28 and 42, the bone surface area (BS) and the bone volume (BV) for 15% (w/v) hydrogels were shown to be significantly higher than that of untreated and 7% (w/v) groups (Fig. 6B, C). For instance, at day 42, the BS for 15% (w/v) hydrogels corresponded to $2.96 \pm 0.46\ mm^2$, which was significantly higher than the untreated controls (i.e., $1.03 \pm 0.63\ mm^2$) and 7% (w/v) hydrogels (i.e., $1.40 \pm 0.53\ mm^2$) (Fig. 6B). Moreover, the highest BV was observed for 15% (w/v) bioadhesives (i.e., 7.16 ± 1.65 mm), which was significantly higher than those of untreated (i.e., $2.76 \pm 1.03\ mm^3$) and 7% (w/v) bioadhesives (i.e., $4.45 \pm 0.72\ mm^3$) (Fig. 6C). Statistical analysis

indicated that both the concentration of the biopolymer and the treatment time had a significant effect on BV and BS. For instance, the BS and BV increased 1.27 and 1.66-fold respectively, at 28 and 42 days post-procedure, which was indicative of sustained bone regeneration throughout the experiment (Fig. 6B, C).

The higher degree of bone regeneration observed for 15% (w/v) bioadhesive could be due in part to the direct contribution of the enhanced mechanical properties of hydrogels with higher polymer concentrations [36]. For instance, Huebsch *et al.* demonstrated that the contribution of matrix elasticity to new bone formation *in vivo* is highly correlated with mechanically induced osteogenesis [36]. They reported that the BV and mineral density obtained for hydrogels with elasticities in the range of 60 kPa was significantly higher than those with 5 kPa or 120 kPa moduli [36] In our study, 15% (w/v) bioadhesives, which exhibited elastic and compressive modulus corresponding to 53.0 ± 10.3 kPa and 52.2 ± 4.7 kPa (Fig. 1B), respectively, could potentially enable mechanically induced osteogenesis and thus, promote the formation of new bone *in vivo*. However, the clinical efficacy of antimicrobial bioadhesives for the treatment of patients with advanced PI could be limited due to the lack of a bona fide osteoinductive strategy. Although previous groups have reported the development of regenerative bioadhesives, they often rely on the use of growth factors [50; 51], stem cells [36; 52], and other bioactive molecules [53; 54]. These methods often suffer from clinical limitations and drawbacks [55; 56]. Due to these limitations, in our future work we will introduce a cell/growth factor-free strategy by the incorporation of alternative osteoinductive strategies such as nanosilicates [57] into antimicrobial bioadhesives which could constitute an attractive platform for the development of osteoinductive and antimicrobial bioadhesives for the treatment of PIDs.

3. Conclusion

The clinical management of PIDs still constitutes a significant challenge for clinicians and researchers in the dentistry field. In this study, we engineered antimicrobial hydrogel bioadhesives for the treatment of PIDs. The hydrogel precursors could be readily delivered and photocrosslinked *in situ* using commercial dental curing systems. These bioadhesives exhibited tunable mechanical stiffness and elasticity, and comparatively higher adhesive strength to implant and oral surfaces than commercial adhesives. In addition, the bioadhesives showed high antimicrobial activity *in vitro* against *P. gingivalis*, a pathogenic bacterium associated with the onset and progression of PIDs. *In vitro* and *ex vivo* studies demonstrated that the bioadhesives were highly cytocompatible and could provide a suitable microenvironment for migratory stromal cells deployed from encapsulated bone sutures. Furthermore, *in vivo* studies showed that the bioadhesives could promote bone regeneration by supporting the growth of migratory progenitor cells. Taken together, our results demonstrated the remarkable potential of our bioadhesive hydrogels to be used as adhesive, antimicrobial, and cell-supportive barriers that can support tissue healing and bone regeneration *in vivo* for the treatment of PIDs.

4. EXPERIMENTAL

4.1. Synthesis of photocrosslinkable bioadhesive prepolymers

Gelatin methacryloyl was synthesized as previously described [58–60]. Briefly, 10 g gelatin from cold water fish skin (Sigma-Aldrich) was dissolved in 100 ml DPBS at 60 °C for 30 min. Next, 8% (v/v) methacrylic anhydride (Sigma-Aldrich) was added to the solution drop-wise under vigorous stirring at 60 °C for another 3 h. The solution was then diluted with 300 ml DPBS to stop the reaction and dialyzed (Spectrum Laboratories, MWCO = 12–14 kDa) in a deionized water bath at 50 °C for 5 days to remove the unreacted methacrylic anhydride. The resulting solution was filtered and lyophilized for 4 days.

4.2. Fabrication of bioadhesive hydrogels

Adhesive hydrogels (Gel) were formed by first dissolving different concentrations of gelatin methacryloyl (7 and 15% (w/v)) in the photoinitiator solution containing triethanolamine (TEA, 1.88% (w/v)) and N-vinyl caprolactam (VC, 1.25% (w/v)) in distilled water at room temperature. A separate solution of Eosin Y disodium salt (0.5 mM) was also prepared in distilled water. The biopolymer/TEA/VC solutions were then mixed with Eosin Y prior to crosslinking to form the final precursor solution. To form the hydrogels, 70 mL of the precursor solution was pipetted into polydimethylsiloxane (PDMS) cylindrical molds (diameter: 6 mm; height: 2.5 mm) for compressive tests, or rectangular molds (12 × 5 × 1 mm) for tensile tests. Lastly, the solutions were photocrosslinked upon exposure to visible light (420–480 nm) for 120 s, using a VALO dental light curing unit (Ultradent Products, Inc.). GelAMP hydrogels were formed by dissolving 0.2 %(w/v) AMP Tet213 (CSC Scientific, Inc.) in TEA/VC/Eosin Y photoinitiator solution. The lyophilized biopolymers were then dissolved in the resulting solution and photocrosslinked as described before.

4.3 Mechanical properties

The tensile and compressive properties of the hydrogel adhesives were evaluated using an Instron 5542 mechanical tester, as described before [25] (Supporting Information, Methods).

4.4. In vitro swellability and degradation

The *in vitro* swellability (24 h) and degradation (14 days) of bioadhesives were performed in DPBS as described before [25] (Supporting Information, Methods).

4.5. In vitro adhesion

In vitro wound closure: Wound closure was performed on both porcine gingiva and skin using a modified ASTM F2458–05 test, as described previously [25]. Briefly, the porcine gingiva was isolated from fresh porcine mandible. Tissues were then cut into 1 × 2 cm pieces and kept moist prior to the test. The tissues were glued onto two pre-cut glass slides (20 mm × 30 mm) and then 50 μL of precursor solution was pipetted and crosslinked using a dental light curing system to form the adhesives. The samples were then placed between the Instron tensile grips and the ultimate adhesive strength was calculated at break ($n \geq 5$). Similarly, 50 μL of the commercial adhesive material was tested as control.

In vitro lap shear: The lap shear strength of the bioadhesives and two commercial adhesives Evicel® (Ethicon, Somerville, NJ, USA) and CoSEAL™ (Baxter, Deerfield, IL, USA) was determined according to a modified ASTM test (F2255–05). Both titanium and glass slides were used as the substrates. Glass slides (10 mm × 30 mm) were coated with gelatin solution and dried at 37 °C. For adhesive tests on titanium, a piece of titanium (10 mm × 10 mm) was attached to a glass slide and 10 μl of the precursor solution was photocrosslinked between the titanium and the gelatin coated glass slide. The lap shear strength of the adhesives was then measured under tensile stress at a rate of 1 mm/min using an Instron mechanical tester. The ultimate stress was reported as shear strength of the bioadhesives ($n \geq 5$). Similarly, 10 μL of the commercial adhesive material was tested as control.

In vitro burst pressure: The burst pressure of the bioadhesives, Evicel®, and CoSEAL™ were determined using a modified ASTM (F2392–04) test as described previously[24]. A piece of porcine intestine was fixed between the stainless-steel annuli of a custom designed burst pressure set up. A 2 mm defect was then created on the center of the tissue. Next, 30 μl precursor solution was applied to the defect site and crosslinked using a dental light curing system. Air pressure was then applied to the sealed tissue and the maximum resistance pressure was recorded as burst pressure ($n \geq 5$). Similarly, 30 μl of the commercial adhesive material was tested as control.

4.6. *In vitro antimicrobial* properties of adhesive hydrogels

P. gingivalis (a clinical isolate A7436 [61]) was used to evaluate the antimicrobial properties of GelAMP bioadhesives. *P. gingivalis* was grown on 5% sheep's blood agar plates supplemented with hemin and vitamin K (H & K) in an anaerobic system (5% H_2, 15% CO_2, 80% N_2) at 37 °C for 7 days. The bacteria colonies were then transferred to Wilkins-Chalgren Anaerobe Broth (Oxoid™) media to prepare a 10^8 CFU/ml bacterial solution. For antimicrobial tests, 1 ml of a 10^8 CFU/ml bacteria solution was seeded on cylindrical hydrogels with and without AMP (0, and 0.2% (w/v) or 1.34 mM) in 24-well plates. After 72 h anaerobic incubation, the samples were removed from the media and washed gently with DPBS 3 times. Next, each sample was placed in 1 ml DPBS and vortexed for 15 min to release bacteria from within the scaffold. The solutions were then logarithmically diluted to 10^{-1}, 10^{-3} and 10^{-4} dilutions. A 30 μl volume of each dilution was then seeded on sheep's blood agar plates with H & K and incubated for 5 days. The number of colonies was counted and reported for each sample ($n = 4$). For SEM imaging, hydrogels were removed from the media and washed 3 times with DPBS. The samples were then fixed in 2.5% (v/v) glutaraldehyde (Sigma-Aldrich) and 4% (v/v) paraformaldehyde (Sigma-Aldrich) in DPBS for 30 min. After fixation, the samples were gently washed 3 times with DPBS and dehydrated using a serially diluted ethanol solution in water (30%, 50%, 70%, 90% and 100% (v/v)). The samples were then dried using a critical point dryer. Lastly, the samples were mounted on aluminum SEM stubs, sputter coated with 6 nm of gold/palladium, and imaged by a Hitachi S-4800 SEM ($n = 3$).

4.7. *In vitro cell* studies

Cell lines: Bone marrow mouse stromal cells (W-20–17) were cultured at 37 °C and 5% CO_2 in Minimum Essential Medium (MEM) Alpha media (Gibco), containing 10% (v/v) fetal bovine serum (FBS) and 1% (v/v) penicillin/streptomycin (Gibco).

2D cell seeding on adhesive hydrogels: Hydrogels were formed by pipetting 7 μl of precursor solution between a 3-(trimethoxysilyl) propyl methacrylate (TMSPMA, Sigma-Aldrich) coated glass slide and a glass coverslip separated with a 100 μm spacer. Bioadhesive hydrogels were photocrosslinked using visible light for 60 sec. The hydrogels were seeded with W-20–17 cells (5×10^6 cells/ml) and kept at 37 °C, 5% CO_2 for 5 days [60]

3D cell encapsulation within the engineered hydrogels: For 3D cell encapsulation, a cell suspension of W-20–17 cells (5×10^6 cells/ml) was prepared by trypsinization and re-suspension in MEM alpha medium. The cell suspension was centrifuged to form a cell pellet and the media was discarded. A hydrogel precursor containing 7% bioadhesive was prepared in culture media containing TEA/VC/Eosin Y and mixed with the cell pellet. Hydrogels were formed by pipetting 7 μl of the precursor solution between a TMSPMA-coated glass slide and a glass coverslip separated with a 100 μm spacer, and photocrosslinking upon exposure to visible light for 60 sec. Lastly, the glass slides with the encapsulated W-20–17 cells were placed in 24 well plates and incubated in MEM alpha at 37 °C and 5% CO_2.

Cell viability proliferation, and spreading: A calcein AM/ethidium homodimer-1 live/dead kit (Invitrogen) was used to evaluate cell viability as described previously [62]. Cell proliferation and metabolic activity was determined using a commercial PrestoBlue assay (Fisher) on days 0, 1, 3 and 5 as described previously[25]. Cell spreading in 2D and 3D cultures was evaluated via fluorescent staining of F-actin microfilaments and cell nuclei [25; 63] (Supporting Information, Methods) ($n \geq 3$).

4.8. Animal studies

Calvarial bone suture tissue extraction and encapsulation into the gels: All animal experiments were performed according to the Guide for the Care and Use of Laboratory Animals (IACUC approval IS00000535) at Harvard School of Dental Medicine. For all experiments, 7–8 weeks-old wild type house mice (Mus musculus) were used. To obtain the calvarial bone sutures, mice were first euthanized by CO_2 inhalation, followed by cervical dislocation. After decapitation, the head was cleaned using 70% ethanol. A cut was then created through the skin at the base of the skull, using a surgical blade. Next, an incision was made starting at the nose bridge and ending at the base of the skull followed by removal of the skin from the top of the head. The calvaria was then cut and transferred to a petri dish with DPBS. After washing with DPBS, the soft tissues were removed using tweezers and the sutures were isolated using scissors. The isolated tissues were chopped into small fragments of 1 – 2 mm^2 and quickly transferred to ice-cold cell culture media prior to use. For encapsulation, the suture fragments were placed on a flat petri dish, in between two spacers (500 μm). Then 70 μl of the bioadhesive precursor was pipetted on the tissue samples and covered by a glass cover slip. The samples were then photocrosslinked for 2 min using a dental curing light. Samples were removed from petri dishes and placed in 12

well tissue culture plates. Next, 2 ml MEM Alpha media, containing 10% (v/v) fetal bovine serum (FBS) and 1% (v/v) penicillin/streptomycin were added to each well and the samples were incubated at 37 °C for up to 30 days. The samples were imaged using a Zeiss Primo Vert inverted microscope, and the cell metabolic activity was evaluated as described before ($n \geq 3$).

Mouse calvarial bone defect model: Male and female mice were assigned randomly to all experimental groups. After general anesthesia, 2-mm round defects were made with surgical bur on right and left parietal bone of mice. Next, 10 μl of the precursor solution were injected in the defect sites (7% and 15% (w/v)) and photopolymerized using a dental light curing unit for 1 min. After anatomical wound closure, the animals recovered from anesthesia. At each time point, the animals were euthanized by CO_2 inhalation, followed by cervical dislocation. After euthanasia, calvarial tissues were collected for μCT and histological analysis (Supporting Information, Methods) ($n \geq 3$).

4.9. Statistical analysis

All data were presented as mean ± standard deviation (*$p < 0.05$, **$p < 0.01$, ***$p < 0.001$ and ****$p < 0.0001$). T-test, one-way, or two-way ANOVA followed by Tukey's test were performed using the GraphPad Prism 6.0 Software.

Supplementary Material

Refer to Web version on PubMed Central for supplementary material.

ACKNOWLEDGEMENTS

The authors thank Katarzyna Wilk and Sasan Ghaffarigarakani for training for histopathological analysis and *in vivo* experiments. N.A. acknowledges the support from C-DOCTOR (Center for Dental, Oral, & Craniofacial Tissue & Organ Regeneration), and National Institutes of Health (NIH) (R01EB023052; R01HL140618).

References:

1. Poli PP, Cicciu M, Beretta M, and Maiorana C. (2017). Peri-implant mucositis and peri-implantitis: A Current understanding of their diagnosis, clinical implications, and a report of treatment using a combined therapy approach. Journal of Oral Implantology 43, 45–50. [PubMed: 27759503]
2. Berglundh T, Armitage G, Araujo MG, Avila-Ortiz G, Blanco J, Camargo PM, Chen S, Cochran D, Derks J, and Figuero E. (2018). Peri -implant diseases and conditions: Consensus report of workgroup 4 of the 2017 World Workshop on the Classification of Periodontal and Peri -Implant Diseases and Conditions. Journal of clinical periodontology 45, S286–S291. [PubMed: 29926491]
3. Renvert S, Persson GR, Pirih FQ, and Camargo PM (2018). Peri -implant health, peri -implant mucositis, and peri -implantitis: Case definitions and diagnostic considerations. Journal of clinical periodontology 45, S278–S285. [PubMed: 29926496]
4. (2013).Peri-implant mucositis and peri-implantitis: a current understanding of their diagnoses and clinical implications. J Periodontol 84, 436–443. [PubMed: 23537178]
5. Costa FO, Takenaka-Martinez S, Cota LO, Ferreira SD, Silva GL, and Costa JE (2012). Peri-implant disease in subjects with and without preventive maintenance: a 5-year follow-up. J Clin Periodontol 39, 173–181. [PubMed: 22111654]
6. Renvert S, Roos-Jansaker AM, and Claffey N. (2008). Non-surgical treatment of peri-implant mucositis and peri-implantitis: a literature review. J Clin Periodontol 35, 305–315.

7. Mombelli A, Feloutzis A, Bragger U, and Lang NP (2001). Treatment of peri-implantitis by local delivery of tetracycline. Clinical, microbiological and radiological results. Clinical oral implants research 12, 287–294. [PubMed: 11488856]
8. Renvert S, Roos -Jansåker AM, and Claffey N. (2008). Non -surgical treatment of peri -implant mucositis and peri -implantitis: a literature review. Journal of Clinical Periodontology 35, 305–315.
9. Grusovin MG, Coulthard P, Worthington HV, George P, and Esposito M. (2010). Interventions for replacing missing teeth: maintaining and recovering soft tissue health around dental implants. Cochrane Database Syst Rev, CD003069.
10. Diz P, Scully C, and Sanz M. (2013). Dental implants in the medically compromised patient. Journal of Dentistry 41, 195–206. [PubMed: 23313715]
11. Esposito M, Coulthard P, Oliver R, Thomsen P, and Worthington H. (2003). Antibiotics to prevent complications following dental implant treatment. The Cochrane Library.
12. Frederic LJ, Michel B, and Selena T. (2018). Oral Microbes, Biofilms and Their Role in Periodontal and Peri-Implant Diseases. Materials (Basel) 11.
13. Derks J, and Tomasi C. (2015). Peri-implant health and disease. A systematic review of current epidemiology. J Clin Periodontol 42 Suppl 16, S158–171.
14. Kinane DF (2001). Causation and pathogenesis of periodontal disease. Periodontol 2000 8–20.
15. Heitz-Mayfield LJA, and Salvi GE (2018). Peri-implant mucositis. J Periodontol 89 Suppl 1, S257–S266.
16. Gottlow J, Nyman S, Karring T, and Lindhe J. (1984). New attachment formation as the result of controlled tissue regeneration. J Clin Periodontol 11, 494–503. [PubMed: 6384274]
17. Nyman S. (1991). Bone regeneration using the principle of guided tissue regeneration. J Clin Periodontol 18, 494–498. [PubMed: 1890234]
18. Ivanovski S, Vaquette C, Gronthos S, Hutmacher DW, and Bartold PM (2014). Multiphasic scaffolds for periodontal tissue engineering. J Dent Res 93, 1212–1221. [PubMed: 25139362]
19. Sheikh Z, Qureshi J, Alshahrani AM, Nassar H, Ikeda Y, Glogauer M, and Ganss B. (2017). Collagen based barrier membranes for periodontal guided bone regeneration applications. J Odontology 105, 1–12.
20. Larsson L, Decker AM, Nibali L, Pilipchuk SP, Berglundh T, and Giannobile WV (2016). Regenerative Medicine for Periodontal and Peri-implant Diseases. J Dent Res 95, 255–266. [PubMed: 26608580]
21. Sam G, and Pillai BR (2014). Evolution of Barrier Membranes in Periodontal Regeneration-"Are the third Generation Membranes really here?". J Clin Diagn Res 8, ZE14–17. [PubMed: 25654055]
22. Sculean A, Nikolidakis D, Nikou G, Ivanovic A, Chapple IL, and Stavropoulos A. (2015). Biomaterials for promoting periodontal regeneration in human intrabony defects: a systematic review. Periodontol 2000 68, 182–216.
23. Kao RT, Nares S, and Reynolds MA (2015). Periodontal regeneration – intrabony defects: a systematic review from the AAP Regeneration Workshop. J Periodontol 86, S77–104. [PubMed: 25216204]
24. Annabi N, Rana D, Shirzaei Sani E, Portillo-Lara R, Gifford JL, Fares MM, Mithieux SM, and Weiss AS (2017). Engineering a sprayable and elastic hydrogel adhesive with antimicrobial properties for wound healing. Biomaterials 139, 229–243. [PubMed: 28579065]
25. Shirzaei Sani E, Portillo-Lara R, Spencer A, Yu W, Geilich BM, Noshadi I, Webster TJ, and Annabi N. (2018). Engineering Adhesive and Antimicrobial Hyaluronic Acid/Elastin-like Polypeptide Hybrid Hydrogels for Tissue Engineering Applications. ACS Biomaterials Science & Engineering.
26. Athirasala A, Tahayeri A, Thrivikraman G, Franca CM, Monteiro N, Tran V, Ferracane J, and Bertassoni LE (2018). A dentin-derived hydrogel bioink for 3D bioprinting of cell laden scaffolds for regenerative dentistry. Biofabrication 10, 024101.
27. Monteiro N, Thrivikraman G, Athirasala A, Tahayeri A, França CM, Ferracane JL, and Bertassoni LE (2018). Photopolymerization of cell-laden gelatin methacryloyl hydrogels using a dental curing light for regenerative dentistry. Dental Materials 34, 389–399. [PubMed: 29199008]

28. Sinha RP, and Hader D-P (2002). UV-induced DNA damage and repair: a review. Photochemical & Photobiological Sciences 1, 225–236. [PubMed: 12661961]
29. Kappes UP, Luo D, Potter M, Schulmeister K, and Runger TM (2006). Short-and long-wave UV light (UVB and UVA) induce similar mutations in human skin cells. Journal of Investigative Dermatology 126, 667–675. [PubMed: 16374481]
30. Wang Z, Abdulla R, Parker B, Samanipour R, Ghosh S, and Kim K. (2015). A simple and high-resolution stereolithography-based 3D bioprinting system using visible light crosslinkable bioinks. Biofabrication 7, 045009.
31. Assmann A, Vegh A, Ghasemi-Rad M, Bagherifard S, Cheng G, Sani ES, Ruiz-Esparza GU, Noshadi I, Lassaletta AD, Gangadharan S, et al. (2017). A highly adhesive and naturally derived sealant. Biomaterials 140, 115–127. [PubMed: 28646685]
32. Soucy JR, Shirzaei Sani E, Portillo Lara R, Diaz D, Dias F, Weiss AS, Koppes AN, Koppes RA, and Annabi N. (2018). Photocrosslinkable Gelatin/Tropoelastin Hydrogel Adhesives for Peripheral Nerve Repair. Tissue Engineering Part A.
33. Shih H, and Lin CC (2013). Visible -light -mediated thiol -Ene hydrogelation using eosin -Y as the only photoinitiator. Macromolecular rapid communications 34, 269–273. [PubMed: 23386583]
34. Noshadi I, Hong S, Sullivan KE, Shirzaei Sani E, Portillo-Lara R, Tamayol A, Shin SR, Gao AE, Stoppel WL, Black Iii LD, et al. (2017). In vitro and in vivo analysis of visible light crosslinkable gelatin methacryloyl (GelMA) hydrogels. Biomater Sci.
35. Kazemzadeh-Narbat M, Kindrachuk J, Duan K, Jenssen H, Hancock RE, and Wang R. (2010). Antimicrobial peptides on calcium phosphate-coated titanium for the prevention of implant-associated infections. Biomaterials 31, 9519–9526. [PubMed: 20970848]
36. Huebsch N, Lippens E, Lee K, Mehta M, Koshy ST, Darnell MC, Desai RM, Madl CM, Xu M, and Zhao X. (2015). Matrix elasticity of void-forming hydrogels controls transplanted-stem-cell-mediated bone formation. Nature materials 14, 1269. [PubMed: 26366848]
37. Peh KK, and Wong CF (1999). Polymeric films as vehicle for buccal delivery: swelling, mechanical, and bioadhesive properties. J Pharm Pharm Sci 2, 53–61. [PubMed: 10952770]
38. Nasajpour A, Ansari S, Rinoldi C, Rad AS, Aghaloo T, Shin SR, Mshra YK, Adelung R, Swieszkowski W, and Annabi N. (2018). A multifunctional polymeric periodontal membrane with osteogenic and antibacterial characteristics. Advanced Functional Materials 28, 1703437.
39. Cheng H, Yue K, Kazemzadeh-Narbat M, Liu Y, Khalilpour A, Li B, Zhang YS, Annabi N, and Khademhosseini A. (2017). Mussel-Inspired Multifunctional Hydrogel Coating for Prevention of Infections and Enhanced Osteogenesis. ACS Applied Materials & Interfaces.
40. Purk JH, Healy M, Dusevich V, Glaros A, and Eick J.D.J.T.J.o.t.A.D.A (2006). In vitro microtensile bond strength of four adhesives tested at the gingival and pulpal walls of Class II restorations. 137, 1414–1418.
41. Sofan E, Sofan A, Palaia G, Tenore G, Romeo U, and Migliau G.J.A.d.s. (2017). Classification review of dental adhesive systems: from the IV generation to the universal type. 8, 1.
42. Khurshid Z, Zafar MS, Naseem M, Khan RS, and Najeeb S. (2018). Human Oral Defensins Antimicrobial Peptides: A Future Promising Antimicrobial Drug. Curr Pharm Des 24, 1130–1137. [PubMed: 29611481]
43. Mallapragada S, Wadhwa A, and Agrawal P. (2017). Antimicrobial peptides: The miraculous biological molecules. J Indian Soc Periodontol 21, 434–438. [PubMed: 29551860]
44. Shi J, Liu Y, Wang Y, Zhang J, Zhao S, and Yang G. (2015). Biological and immunotoxicity evaluation of antimicrobial peptide-loaded coatings using a layer-by-layer process on titanium. Scientific reports 5, 16336. [PubMed: 26548760]
45. Chen J, Zhu Y, Song Y, Wang L, Zhan J, He J, Zheng J, Zhong C, Shi X, and Liu SJJo.M.C.B. (2017). Preparation of an antimicrobial surface by direct assembly of antimicrobial peptide with its surface binding activity. 5, 2407–2415.
46. Thies RS, Bauduy M, Ashton BA, Kurtzberg L, Wozney JM, and Rosen V. (1992). Recombinant human bone morphogenetic protein-2 induces osteoblastic differentiation in W-20–17 stromal cells. Endocrinology 130, 1318–1324. [PubMed: 1311236]
47. Maruyama T, Jeong J, Sheu T-J, and Hsu W. (2016). Stem cells of the suture mesenchyme in craniofacial bone development, repair and regeneration. Nature communications 7, ncomms10526.

48. Wilk K, Yeh S-CA, Mortensen LJ, Ghaffarigarakani S, Lombardo CM, Bassir SH, Aldawood ZA, Lin CP, and Intini G. (2017). Postnatal calvarial skeletal stem cells expressing PRX1 reside exclusively in the calvarial sutures and are required for bone regeneration. Stem cell reports 8, 933–946. [PubMed: 28366454]
49. Wahid F, Zhong C, Wang H-S, Hu X-H, and Chu L-QJP (2017). Recent advances in antimicrobial hydrogels containing metal ions and metals/metal oxide nanoparticles.9, 636.
50. Patterson J, Siew R, Herring SW, Lin AS, Guldberg R, and Stayton PS (2010). Hyaluronic acid hydrogels with controlled degradation properties for oriented bone regeneration. Biomaterials 31, 6772–6781. [PubMed: 20573393]
51. Gibbs DM, Black CR, Dawson JI, and Oreffo RO (2016). A review of hydrogel use in fracture healing and bone regeneration. Journal of tissue engineering and regenerative medicine 10, 187–198. [PubMed: 25491789]
52. Chamieh F, Collignon A-M, Coyac BR, Lesieur J, Ribes S, Sadoine J, Llorens A, Nicoletti A, Letourneur D, and Colombier M-L (2016). Accelerated craniofacial bone regeneration through dense collagen gel scaffolds seeded with dental pulp stem cells. Scientific reports 6, 38814. [PubMed: 27934940]
53. Nguyen MK, Jeon O, Dang PN, Huynh CT, Varghai D, Riazi H, McMillan A, Herberg S, and Alsberg E. (2018). RNA interfering molecule delivery from in situ forming biodegradable hydrogels for enhancement of bone formation in rat calvarial bone defects. Acta biomaterialia.
54. Kyllonen L, D'Este M, Alini M, and Eglin D. (2015). Local drug delivery for enhancing fracture healing in osteoporotic bone. Acta biomaterialia 11, 412–434. [PubMed: 25218339]
55. Woo EJ (2012). Adverse events reported after the use of recombinant human bone morphogenetic protein 2. Journal of oral and maxillofacial surgery : official journal of the American Association of Oral and Maxillofacial Surgeons 70, 765–767.
56. Mesfin A, Buchowski JM, Zebala LP, Bakhsh WR, Aronson AB, Fogelson JL, Hershman S, Kim HJ, Ahmad A, and Bridwell KH (2013). High-dose rhBMP-2 for adults: major and minor complications: a study of 502 spine cases. The Journal of bone and joint surgery American volume 95, 1546–1553.
57. Wang Y, Cui W, Chou J, Wen S, Sun Y, and Zhang H. (2018). Electrospun nanosilicates-based organic/inorganic nanofibers for potential bone tissue engineering. Colloids Surf B Biointerfaces 172, 90–97. [PubMed: 30142529]
58. Uehara M, Li X, Sheikhi A, Zandi N, Walker B, Saleh B, Banouni N, Jiang L, Ordikhani F, and Dai L.J.S.r. (2019). Anti-IL-6 eluting immunomodulatory biomaterials prolong skin allograft survival. 9, 6535.
59. Walker BW, Lara RP, Yu C, Sani ES, Kimball W, Joyce S, and Annabi NJB (2019). Engineering a naturally-derived adhesive and conductive cardiopatch.
60. Sani ES, Kheirkhah A, Rana D, Sun Z, Foulsham W, Sheikhi A, Khademhosseini A, Dana R, and Annabi N. (2019). Sutureless repair of corneal injuries using naturally derived bioadhesive hydrogels. Science Advances 5, eaav1281.
61. Papathanasiou E, Kantarci A, Konstantinidis A, Gao H, and Van Dyke T. (2016). SOCS-3 regulates alveolar bone loss in experimental periodontitis. Journal of dental research 95, 1018–1025. [PubMed: 27126447]
62. Annabi N, Zhang Y-N, Assmann A, Sani ES, Cheng G, Lassaletta AD, Vegh A, Dehghani B, Ruiz-Esparza GU, and Wang X. (2017). Engineering a highly elastic human protein-based sealant for surgical applications. Science translational medicine 9, eaai7466.
63. Noshadi I, Walker BW, Portillo-Lara R, Shirzaei Sani E, Gomes N, Aziziyan MR, and Annabi N. (2017). Engineering Biodegradable and Biocompatible Bio-ionic Liquid Conjugated Hydrogels with Tunable Conductivity and Mechanical Properties. Sci Rep 7, 4345. [PubMed: 28659629]

A. ASSOCIATED FILES AND FORMS

Progress and Potential statement

Clinical management of peri-implant diseases (PIDs) constitutes significant challenges. Here, we report a multi-functional adhesive hydrogel with antimicrobial properties for treatment of PIDs. The hydrogel precursor can be crosslinked in seconds using commercially available dental curing systems and form a hydrogel that can adhere to both soft tissues (gingiva) and hard tissues (dental implants/bone). The hydrogel was extensively characterized *in vitro*, *ex vivo*, and *in vivo*. The engineered adhesive has high adhesion, mechanical stability, cytocompatibility, antimicrobial properties, biodegradability, and bone regenerative capacity. Overall, this antimicrobial hydrogel adhesive could be used as a minimally invasive platform for the development of more effective therapeutic strategies against PIDs.

Highlights

A visible light crosslinkable hydrogel for treatment of periodontal diseases

High adhesion to soft/hard tissues and implant surfaces

High antimicrobial properties against periodontal pathogenic bacteria

A versatile platform for autologous bone growth *in vivo*

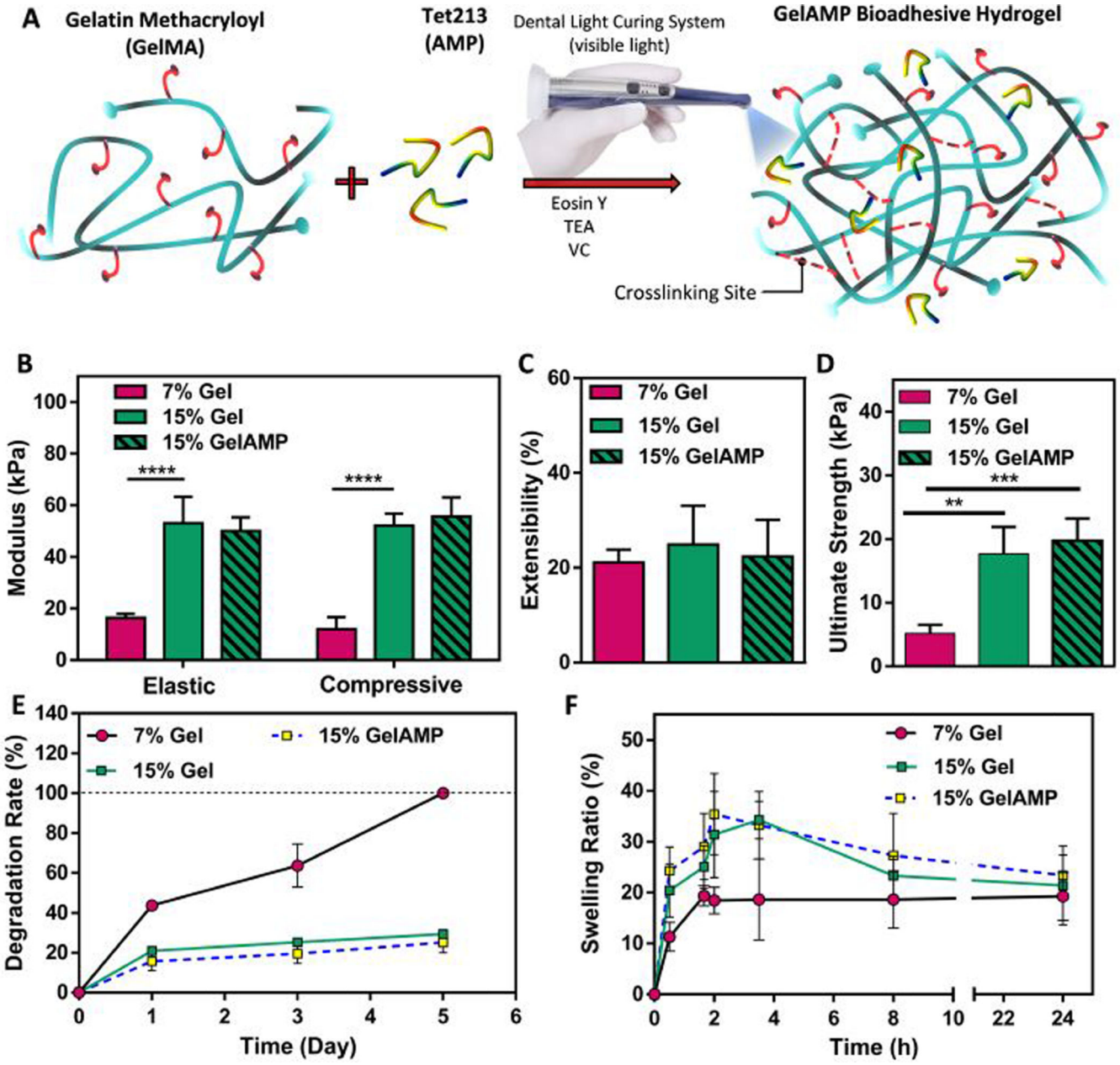

Figure 1. Physical characterization of bioadhesive hydrogels.

(A) Synthesis and photocrosslinking process of bioadhesive hydrogels. **(B)** Elastic and compressive modulus, **(C)** extensibility, and **(D)** ultimate stress of the adhesive hydrogels produced by using 7% and 15% (w/v) total polymer concentration with and without AMP. **(E)** *In vitro* degradation properties in 20 (ig/ml collagenase type II solution in Dulbecco's phosphate buffered saline (DPBS) and **(F)** swelling ratios in DPBS for 7% and 15% (w/v) adhesive hydrogels with and without AMP. Data are represented as mean ± SD (*$p < 0.05$, **$p < 0.01$, ***$p < 0.001$, ****$p < 0.0001$ and $n \geq 5$).

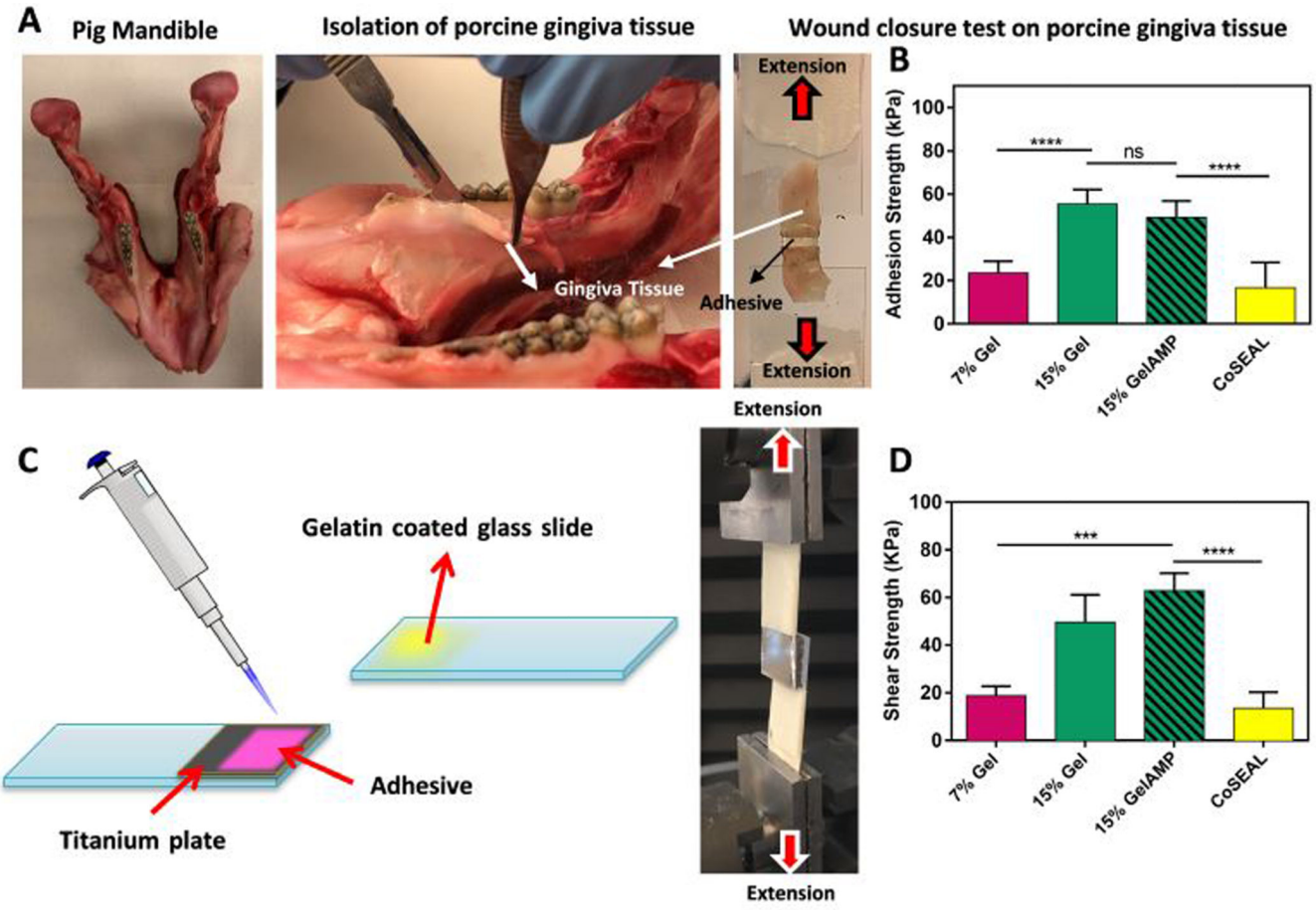

Figure 2. *In vitro* and *ex vivo* adhesion properties of GelAMP hydrogels.

(A) Representative images of wound closure test using pig gingiva tissue based on ASTM standard test (F2458–05) and **(B)** adhesion strength of bioadhesive hydrogels and a commercially available adhesive (CoSEAL™) to porcine gingiva. **(C)** Schematic of the *in vitro* lap shear test based on a modified ASTM standard (F2255–05), using titanium as a substrate. **(D)** The *in vitro* lap shear strength of the bioadhesive hydrogels at 7% and 15% polymer concentration and a commercially available adhesive (CoSEAL™). Data are represented as mean ± SD (**p < 0.01, ***p < 0.001, ****p < 0.0001, n=5).

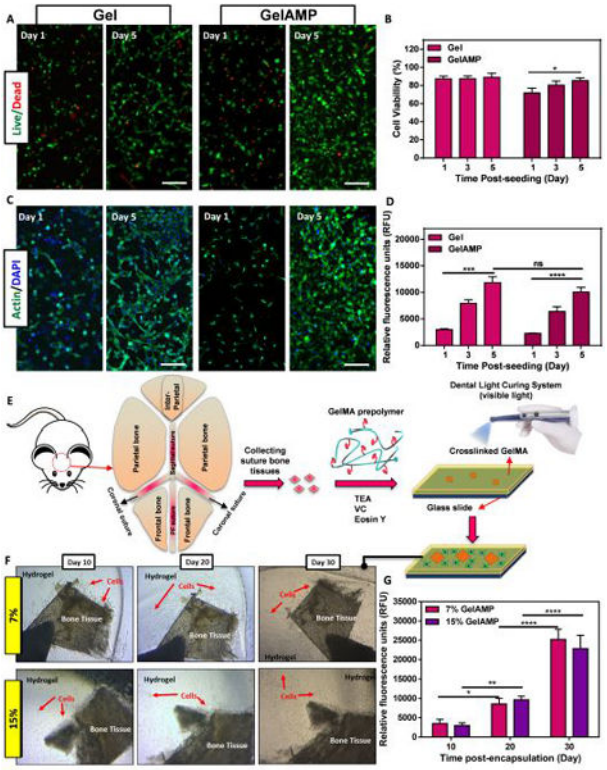

Figure 3. *In vitro* antibacterial properties of bioadhesive hydrogels against *P. gingivalis*.

(A) Representative images of *P. gingivalis* colonies grew on blood agar plates for bioadhesives with and without AMP (Dilution 1, 3 and 4 represent 1-, 3-and 4-logarithmic dilutions respectively). **(B)** Quantification of colony forming units (CFUs) for bioadhesive hydrogels with and without AMP (0.2% (w/v) or 1.34 mM), seeded with *P. gingivalis bacteria* (day 4). Representative scanning electron microscope (SEM) images of *P. gingivalis* colonization on bioadhesive hydrogels containing **(C)** 0% and **(D)** 0.2% (w/v) AMP. Clusters of bacteria are shown with yellow arrows. (***p < 0.001 and ****p < 0.0001).

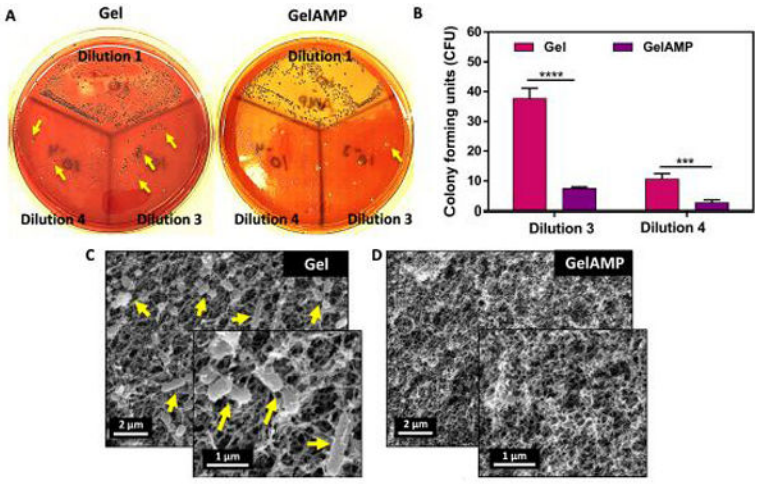

Figure 4. In vitro 3D encapsulation of W-20–17 cells and mouse calvarial bone sutures inside adhesive hydrogels.

(A) Representative live/dead images of W-20–17 cells encapsulated within bioadhesives hydrogels with and without AMP after 1 and 5 days. **(B)** Quantification of viability of W-20–17 cells incorporated within hydrogels without (control) and with AMP (GelAMP) using live/dead assays on days 1, 3, and 5 post encapsulation. **(C)** Representative phalloidin (green)/DAPI (blue) stained images of cell-laden bioadhesive with and without AMP after 1 and 5 days. **(D)** Quantification of metabolic activity of W-20–17 cells encapsulated in hydrogels after 1, 3, and 5 days. **(E)** Schematic diagram of the extraction and encapsulation of mouse calvarial bone sutures in 3D hydrogel network. **(F)** Representative images of calvarial bone sutures encapsulated within 7 % and 15% (w/v) bioadhesives to visualize growth and diffusion of cells at days 10, 20 and 30 post encapsulation. **(G)** Quantification of metabolic activity of migratory stromal cells from encapsulated bone sutures. Hydrogels were formed at 120 sec visible light exposure time (** $p < 0.01$, *** $p < 0.001$), **** $p < 0.0001$).

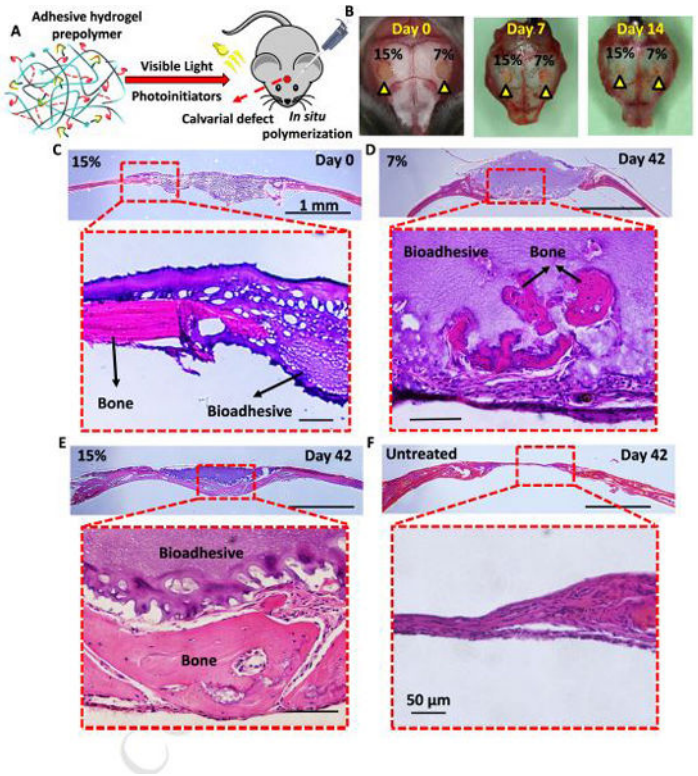

Figure 5. ***In vivo*** **evaluation of bioadhesive hydrogels using a mouse calvarial defect model.**
(A) Schematic diagram of *in situ* application of bioadhesive hydrogels in a mouse calvarial defect model. **(B)** 7% and 15% bioadhesive hydrogels were delivered to artificially created bone defects in mouse calvaria (yellow arrowheads), and photopolymerized for 1 min using a commercially available dental curing light. 7 and 14 days after implantation, samples remained in place, without any sign of detachment. **(C)** Histological evaluation (H&E staining) of the 15% (w/v) bioadhesives at day 0 post implantation. Representative H&E images for **(D)** 7% (w/v) and (E) 15% (w/v) bioadhesive treatment, and **(F)** untreated sample after 42 days post implantation.

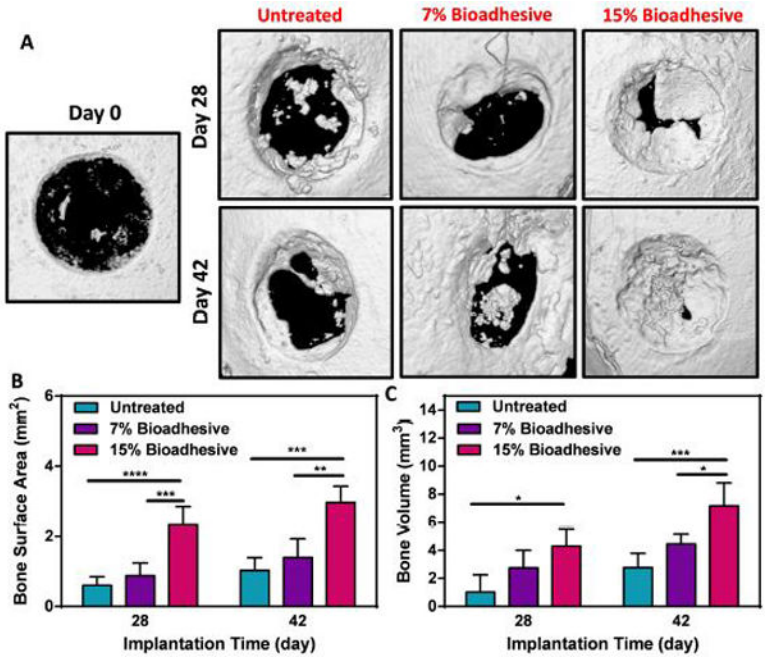

Figure 6. Quantitative evaluation of new bone formation using μCT analysis.

(A) Representative micro-CT images for untreated defect, and defects treated with 7% and 15% bioadhesives on days 28 and 42 post-implantation **(B)** Quantitative analysis of bone surface area and **(C)** and bone volume. Data are represented as mean ± SD (*p < 0.1, **p < 0.01, ***p < 0.001, ****p < 0.0001, n=5).